Metal-Organic Frameworks from Divalent Metals and 1,4-Benzenedicarboxylate with Bidentate Pyridine-N-oxide Co-ligands

Journal:	*Crystal Growth & Design*
Manuscript ID:	cg-2014-01690b.R1
Manuscript Type:	Article
Date Submitted by the Author:	n/a
Complete List of Authors:	Munn, Alexis; University of Warwick, Chemistry Amabilino, Silvia; University of Warwick, Stevens, Thomas; University of Warwick, Daniels, Luke; University of Warwick, Clarkson, Guy; University of Warwick, Chemistry Millange, Franck; Université Versailles, Institut Lavoisier Versailles Lenox, Matthew; University of Edinburgh, Chemical Engineering Düren, Tina; University of Bath, Chemical Engineering Bourrelly, Sandrine; Aix Marseille UnivsersityMADIREL, Aix Marseille University CNRS UMR7246 Llewellyn, Philip; Aix-Marseille Univ. & CNRS, MADIREL (UMR 7248) Walton, Richard; University of Warwick, Department of Chemistry

Metal-Organic Frameworks from Divalent Metals and 1,4-Benzenedicarboxylate with Bidentate Pyridine-*N*-oxide Co-ligands

Alexis S. Munn,[1] Silvia Amabilino,[1] Thomas W. Stevens,[1] Luke M. Daniels,[1] Guy J. Clarkson,[1] Franck Millange,[2] Matthew J. Lennox,[3] Tina Düren,[3‡] Sandrine Bourelly,[4] Philip Llewellyn[4] and Richard I. Walton[1,*]

1. Department of Chemistry, University of Warwick, Coventry, CV4 7AL, U.K.

* Author for Correspondence: email: r.i.walton@ warwick.ac.uk

2. Institut Lavoisier Versailles, Université de Versailles, UMR 8180, 78035 Versailles, France

3. Institute for Materials and Processes, School of Engineering, The University of Edinburgh The King's Buildings, Edinburgh, EH9 3JL, U.K.

4. Aix-Marseille University, Laboratoire MADIREL, UMR CNRS 7246, Centre de St Jérôme, 13397 Marseille Cedex 20, France

‡ Present address: Department of Chemical Engineering, University of Bath, Claverton Down Bath, BA2 7AY, U.K.

Abstract

Two Co^{2+} metal-organic framework materials, constructed from a combination of 1,4-benzenedicarboxylate (BDC) and either 2,2'-dipyridyl-*N*-oxide (DPNO) or 2,2'-dipyridyl-*N*,*N*'-dioxide (DPNDO), are synthesised under solvothermal reaction conditions and their structures solved by single crystal X-ray diffraction. Both have three-dimensional structures that contain octahedral Co^{2+} centres with μ_2-(η^2) -BDC, and bidentate DPNO or DPNDO co-ligands that bridge pairs of metal centres but do not contribute towards the overall connectivity of the framework. $Co_3(BDC)_3(DPNO)_2$ contains trimers of *trans* corner-shared Co-centred octahedra with one type of bridging BDC ligand forming terminal edges of the trimers, bridging to neighbouring trimer units, and a second type, bridging pairs of metals and also connecting neighbouring trimers. $Co_2(BDC)_2(DPNDO)$ is constructed from one-dimensional inorganic chains consisting of *cis*- and *trans*-corner shared Co^{2+}-centred octahedral. The DPNDO ligand is *bis*-bidentate, forming the edges of one type of octahedron and the *trans* corners of the second type, with the coordination for both octahedra completed by bridging BDC linkers, which in turn connect the inorganic chains to yield a three-dimensional structure. Thermogravimetric analysis shows both materials contain trapped solvent, and while $Co_3(BDC)_3(DPNO)_2$ is unstable with respect to solvent loss, $Co_2(BDC)_2(DPNDO)$, and its magnesium analogue, can be desolvated to yield permanently porous materials that show thermal stability up to 300 °C. For $Co_2(BDC)_2(DPNDO)$, gas adsorption studies show permanent microporosity with moderate uptake of small gas molecules (N_2, CO_2, CH_4 and C_2H_6), supported by Grand Canonical Monte Carlo calculations based on the assumption of rigid crystal structures, while gravimetric analysis shows rapid and reversible methanol adsorption at ambient pressure for both the Co and Mg analogues of the framework.

Introduction

A multi-ligand strategy in the synthesis of coordination polymers naturally leads to greater structural diversity than for single ligand materials, and allows introduction of more than one type of chemical functionality; this is therefore a powerful way to discover new materials that may present new structures and properties that are tuned for desired applications.[1] Such multicomponent, or multivariate materials, can either be considered solid-solutions of end members, each representing a single-ligand MOF,[2] or may have novel structures based on a unique combination of distinct ligands. In the case of porous metal-organic frameworks their adsorption properties are of interest and multi-ligand synthesis has recently allowed access to some striking new families of materials: for example, Yaghi and co-workers have shown enhanced CO capture in a multivariate version of MOF-5 compared to its single ligand equivalents,[3] while several groups have shown how the inclusion of moderating, non-bridging ligands allows the porosity of certain MOFs to be tuned, leading to the idea of a defective linker strategy for controlled porosity.[4,5,6,7] In the cases where two distinct ligand types are used, novel framework architectures can be produced: for example, Hupp and co-workers combined carboxylates with pyridines to form unique structures where the robust carboxylate linkers stabilise pyridine-linked metals against structural collapse, to give materials with permanent porosity and redox activity.[8]

Ligands containing pyridine-*N*-oxide functionalities are known from classical coordination chemistry to coordinate to a variety of metals through oxygen,[9] and have been used recently to form some interesting coordination polymers. For example, Sharma *et al.*, have prepared a range of coordination polymers for diverse metals using pyridine-*N*-oxides in combination with various metals and carboxylate ligands: this includes infinite Mn(II) chains connected by oxygen coordinated μ_2- pyridine-*N*-oxide and with monodentate carboxylate ligands, [10] infinite chain structures of Pb(II),[11] a set of materials based on Group 12 metals,[12] and lanthanide materials which show different binding modes for the pyridine-*N*-oxide.[13,14] In this paper we consider the synthesis of coordination polymers constructed from a combination of one of the simplest, and most widely used, bridging dicarboxylates, 1,4-benzene

dicarboxylate (BDC) with bidentate ligands containing pyridine-*N*-oxide functionalities. Our work has been inspired by that of Xu *et al.*,[15] who used pyridine-*N*-oxides with 1,4-benzene dicarboxylate and Mn^{2+} to form analogues of the well-known framework MIL-53, in which infinite chains of octahedral metal centres, linked by *trans* corner-sharing, form a flexible porous structure by virtue of the cross linking 1,4-benzene dicarboxylates. When pyridine-*N*-oxide is used as a co-ligand in this system its oxygen provides the μ_2 link between adjacent divalent metals (rather than the anionic hydroxide or fluoride in the parent MIL-53 structure that includes trivalent metals[16]) and the pyridine rings fill the pore volume. We extended the work to include the metals Co^{2+} and Ni^{2+} (and mixtures of these metals),[17] and in the case of Co^{2+} showed that by adding substituents to the pyridine ring of pyridine-*N*-oxide, the framework structure could be distorted with retention of the overall topology, by virtue of the steric requirements of the substituent.[18] Xu *et al.* also used 4,4'-dipyridyl-*N*,*N*'-dioxide, itself a bridging bidentate ligand, in combination with 1,4-benzene dicarboxylate to produce a novel MIL-53-like structure in which the bidentate co-ligand was arranged parallel to the dicarboxylate rings so to maintain porosity in an expanded, permanently porous structure.[15]

In the present work we have selected the ligands, 2,2'-dipyridyl-*N*-oxide (DPNO) and 2,2'-dipyridyl-*N*,*N*'-dioxide (DPNDO), Figure 1, and investigated their use in combination with the widely used 1,4-benzenedicarboxylate ligand for the crystallisation of coordination polymers. These bidentate pyridine-*N*-oxides have previously received little attention for the formation of coordination polymers: to our knowledge, only the latter has been used in the formation of infinitely connected coordination compounds for Co^{2+} and Cu^{2+} materials with bridging tricyanomethanide ligands to give infinite chains,[19] a Pb^{2+} iodide with an infinite chain of iodide-edge-shared octahedral and pendant DPNDO completing the metal coordination,[20] and Cu^{2+} materials containing paddle-wheel dimeric units.[21] In each of those examples the 2,2'-dipyridyl-*N*,*N*'-dioxide coordinates through both oxygen donors, but whereas in the first two it coordinates to a single metal, forming the edge of an octahedron, only in the last case does it span two metal centres, to link Cu^{2+} dimers to give an infinite chain.[21] The ligand 2,2'-dipyridyl-*N*-oxide, in contrast, offers the possibility of coordination through nitrogen as well as through

oxygen. We have thus prepared two unique, three-dimensional frameworks containing Co^{2+}, $Co_3(BDC)_3(DPNO)_2$ and $Co_2(BDC)_2(DPNDO)$ whose structures and thermal behaviour are reported herein. For the latter material, which shows stability on desolvation, we have also prepared an Mg^{2+} analogue and studied the behaviour of the two structures toward various adsorbates.

Experimental Section

$Co_3(BDC)_3(DPNO)_2$ was synthesised under solvothermal conditions from $Co(NO_3)_2{\cdot}6H_2O$ (Sigma-Aldrich > 98 %), 1,4-benzenedicarboxylic acid (Sigma-Aldrich > 98 %) and 2,2'-dipyridyl-*N*-oxide (Sigma-Aldrich 98 %) in the molar ratio 1:2:2, respectively, using 0.2 g of $Co(NO_3)_2{\cdot}6H_2O$ dissolved in 10 mL *N*,*N*-dimethyl formamide (DMF) to give a Co^{2+} concentration of 0.07 M. The mixture was thoroughly stirred before heating in a sealed, 20 mL, Teflon-lined autoclave at 90 °C for 2 days. $Co_2(BDC)_2(DPNDO)$ was also synthesised under solvothermal conditions, in this case from $Co(NO_3)_2{\cdot}6H_2O$, 1,4-benzenedicarboxylic acid and 2,2'-dipyridyl-*N*,*N*'-dioxide (Sigma-Aldrich 98 %) in the molar ratio 1:2:2, respectively, using 0.2 g of $Co(NO_3)_2{\cdot}6H_2O$ dissolved in 10 mL of a 1:4 mixture (by volume) of DMF:methanol, to give the same Co^{2+} concentration. In this case crystallisation was performed at 100 °C for 7 days. The magnesium analogue, $Mg_2(BDC)_2(DPNDO)$, was prepared in a similar manner but with the cobalt salt replaced by $Mg(NO_3)_2{\cdot}6H_2O$ (Merck > 99%) and using a higher dilution: 0.03 M Mg^{2+} in 10 mL of a 1:4 mixture of DMF:methanol.

Suitable single crystals for structure determination were selected for each of the cobalt materials and were mounted on glass fibres with silicon grease on a Xcalibur, Gemini diffractometer with a Ruby CCD detector, or using the EPSRC Crystallographic Service,[22] where a Rigaku Saturn724+ diffractometer was used. Using Olex2,[23] the structures were solved with the ShelXS[24] structure solution program using Direct Methods and refined with the ShelXL[24] refinement package using least squares minimisation. $Co_3(BDC)_3(DPNO)_2$ was found to be X-ray sensitive, which may be related to the ease of collapse of the structure upon desolvation (see below), and its structure could only be determined at 100 K.

$Co_2(BDC)_2(DPNDO)$ was much more robust and was studied both at room temperature and as a methanol exchanged form (produced by soaking the crystals in methanol for at least 3 days) at 150 K to prevent subsequent methanol loss. Structure determination details and crystallographic data are shown in Table 1.

Powder X-ray diffraction (Siemens D5000 operating with Cu $K\alpha_{1/2}$ radiation) was measured at room temperature from samples of both Co^{2+} materials, and the magnesium material. *In situ* powder X-ray diffraction with heating (Bruker D8 operating with Cu $K\alpha_{1/2}$ radiation and an Anton Parr HTK900 sample chamber) was recorded from samples of $Co_2(BDC)_2(DPNDO)$ and $Mg_2(BDC)_2(DPNDO)$ to examine the possibility of structural changes with heating and their ultimate thermal stability.

TGA-DSC was recorded under static air from all three materials from room temperature to 1000 °C using a Mettler-Toledo TGA/DSC 1 Star^e System using ~10 mg of material held in an alumina crucible. In separate TGA-DSC experiments, samples of $Co_2(BDC)_2(DPNDO)$ and $Mg_2(BDC)_2(DPNDO)$ that had previously been washed in methanol were each heated to 250 °C before cooling and a flow of nitrogen saturated with methanol vapour introduced, achieved by bubbling the inlet gas through a methanol-filled Drechsel bottle. The mass was monitored throughout and after reaching equilibrium, the samples were heated to 100 °C to then drive off the methanol. A calibration was performed by performing a background scan on an empty crucible under identical conditions.

Nitrogen adsorption isotherms were recorded at 77 K from $Co_2(BDC)_2(DPNDO)$ and $Mg_2(BDC)_2(DPNDO)$ after degassing under vacuum at 150 °C using a BEL Japan, BELSORP Prep instrument. Gas adsorption measurements at 303 K and up to 20 bar were made with CO_2, CH_4, N_2 and C_2H_6 using an in-house built high-throughput instrument at Aix-Marseille University.[25] In this apparatus gas adsorption is measured via a manometric gas dosing system on six samples in parallel. The amounts of gas adsorbed are calculated by an equation of state using the Reference Fluid Thermodynamic and Transport Properties (REFPROP) software package 8.0 of the National Institute of Standards and Technology (NIST).[26] Around 100-200

mg of sample is used, and each sample is thermally activated individually *in situ* under primary vacuum at a chosen temperature overnight, before gas adsorption is studied. The gases were obtained from Air Liquide: nitrogen and methane were of 99.9995% purity (N55) and carbon dioxide and ethane were of 99.995% purity (N45). In these experiments the measurements were cycled to investigate the presence of any residual adsorbed gases, but desorption isotherms were not measured.

Simulated pure component adsorption isotherms of N_2 at 77 K and CH_4, C_2H_6 and CO_2 at 303 K in $Co_2(BDC)_2(DPNDO)$ were generated via Grand Canonical Monte Carlo simulations carried out using the MuSiC software package.[27] Input fugacities for the simulations were calculated using the Peng-Robinson equation of state.[28] The MOF was treated as rigid, with framework atoms kept fixed in their crystallographic positions. Sorbate-MOF interactions were described solely via the Lennard-Jones (LJ) 12-6 potential in the case of N_2, CH_4 and C_2H_6, while CO_2-MOF interactions included both LJ and Coulombic contributions. The LJ parameters for framework C, O, H and N atoms were taken from the DREIDING force field.[29] For Co, for which DREIDING parameters were not available, the UFF[30] was used. Partial charges for framework atoms were determined using the EQeq method.[31] LJ potentials and partial charges for the sorbate atoms were taken from the TraPPE force field.[32,33] Sorbate-sorbate interactions for the alkanes were described using only LJ interactions, while N_2-N_2 and CO_2-CO_2 interactions included both an LJ and electrostatic component. All sorbate molecules were considered to be rigid.

Results and Discussion

1. Crystal structures

$Co_3(BDC)_3(DPNO)_2$ is constructed from trimeric inorganic units consisting of three distorted octahedral Co^{2+} centres linked via *trans* oxygens. In the asymmetric unit there are two cobalts (Co3 and Co4) with double multiplicity and two other unique cobalts (Co1 and Co2) with single multiplicity, and this gives two distinct trimers: one Co4-Co1-Co4 and the other Co3-Co2-Co3, Figure 2a, both constructed from the same arrangement of ligands. The central cobalt in each

is coordinated by six oxygens: an equatorial plane made up of four oxygens from four distinct BDC ligands, each of which uses the second oxygen of the carboxylate group to bridge to one of two of the neighbouring terminal octahedra, and two axial oxygens from the oxygens of the pyridine-*N*-oxide functionality of the co-ligand, which form the corner-shared oxygens with the terminal Co centres. Each of the terminal cobalts in each trimer has its coordination completed by a coordinated nitrogen atom of the DPNO and two oxygens of a further, unique BDC that bind through one carboxylate to form an edge of the octahedron.

The presence of Co^{2+} in $Co_3(BDC)_3(DPNO)_2$ is confirmed from bond valence sums[34] that give values of 2.13, 2.13, 1.99 and 1.96, respectively, for Co1, Co2, Co3 and Co4. Analogous trimeric units have been observed in other cobalt(II) coordination polymers with solely oxygen coordinated ligands, and the local Co^{2+} environment in these is similarly slightly distorted from regular octahedral geometry. For example, Poulsen *et al.* reported a Co^{2+} material, along with an analogous Zn^{2+} material, that contained the same trimeric units, linked solely by BDC, but to give a net anionic framework, with charge balanced by extra-framework ethylammonium cations,[35] and very similar materials have been described by others, using different synthesis approaches, and with different counterions.[36,37,38,39] Zou *et al.* also found similar trimeric units in a Co^{2+} material containing thiophene-2,5-dicarboxylic acid, bridging in a similar manner to BDC, but with *N*-coordinated 1,3-bis(4-pyridyl)propane linkers connecting the termini of the trimers.[40]

The trimeric units in $Co_3(BDC)_3(DPNO)_2$ are linked by the bridging BDC ligands to give a neutral, three-dimensionally extended network whose topology is overall connected only by organic bonds (I^0O^3 in the nomenclature of Cheetham *et al.* [41]), Figure 2a. Each trimer is linked to six other trimers: two of these are via BDC with μ_2-(η^2) bonding modes, such that a chain is formed running parallel to the *b*-axis; while crosslinking with μ_2-(μ_2-η^2: η^1) BDC linkers yields the three-dimensional structure. Figure 2b shows a view of the structure along the *a*-axis, which indicates the possibility of porosity in the structure. The one-dimensional channels thus presented are filled with disordered solvent: the Squeeze routine via Platon was used to model

possible solvent in the voids, which calculated a void volume of 1013.8 $Å^3$ per unit cell (36.3% of the cell volume) with electron density corresponding to a combination of 4 DMF molecules and 5 waters.

$Co_2(BDC)_2(DPNDO)$ also presents a neutral three-dimensional structure, but its connectivity is very different from $Co_3(BDC)_3(DPNO)_2$. While the structure also contains octahedral Co(II), the metal centres are linked by corner sharing to give a one-dimensional inorganic chain with alternating *cis*- and *trans*-shared bridging oxygens, Figure 3a. There are two crystallographically distinct Co centres. The *bis*-bidentate 2,2'-dipyridyl-*N*,*N*'-dioxide ligands, bonded through oxygen form edges of Co1-centred octahedra and the shared corner with neighbouring Co2 octahedra. Thus the Co2-centred octahedral have *trans* corners from two distinct dipyridyl-*N*,*N*'-dioxide ligands. The remaining oxygens forming the coordination sphere of each octahedron are those of BDC linkers, each of which uses one carboxylate to bridge a neighbouring Co1 and Co2 pair. Bond valence sums give values of 2.13 and 2.12 for Co1 and Co2, respectively, confirming the presence of Co^{2+}.

The infinite chains are cross-linked by μ_2-(μ_2-η^2: η^1) BDC linkers, Figure 3b. The chain motif in $Co_2(BDC)_2(DPNDO)$ is similar to that seen in other materials reported in the literature, even in cases where very different chemistry is represented; for example, Attfield and co-workers reported fluorinated aluminium phosphonates that contained the same chains, but made up of corner-sharing $[AlO_4F_2]$ octahedra and with alternating *trans* or *cis* pairs of fluorides and the oxygens belonging to the coordinated alkylenebis(phosphonate)s,[42,43,44] and the aluminium MOF known as NOTT-300 has a similar chain connectivity of $[AlO_4(OH)_2]$ octahedra, but with hydroxide groups forming the *cis* connections and with chains linked by a tetracarboxylate.[45] Other MOFs containing octahedral Mg^{2+} [46] and In^{3+} [47] with the same chain connectivity have also been described.

The overall structure of $Co_2(BDC)_2(DPNDO)$ is a three-dimensional network of connectivity I^1O^2 that presents potential channels in one dimension, Figure 4a: the shortest distance between carbon centres of the dipyridyl-*N*,*N*'-dioxide ligands across the diagonal of the pore is 7.41 Å, which between carbon centres of BDC linkers is 8.88 Å. The program

PLATON[48] was used to calculate a 548.1 Å^3 pore volume (34.0% of the volume). Any solvent present in this space must be highly disordered since no solvent or other molecular fragments could be refined satisfactorily in the voids.

The methanol-exchanged sample of $Co_2(BDC)_2(DPNDO)$, studied at 150 K, shows a lower crystal symmetry (triclinic, $P\bar{1}$) but essentially the same framework structure, with little evidence for any framework movement having resulted upon cooling or the methanol washing, Figure 4b. The solvent accessible void space calculated by PLATON in this case was 526.0 Å^3 (33.1% of the volume), illustrating the similarity of the framework structures between room temperature and 150 K. At low temperature the electron density within the pores could be analysed and this allowed location of methanol and some co-adsorbed water to give an empirical formula of $Co_2(BDC)_2(DPNDO)[CH_3OH]_{2.5}[H_2O]_{1.5}$. There is evidence for hydrogen bonding between methanol and an oxygen of a framework carboxylate (oxygen-oxygen contact of 2.95 Å).

Powder X-ray diffraction of the two cobalt materials similarly proved the phase purity of the samples, by comparison with the simulated pattern from the single crystal structures (Supporting Information). In the case of $Co_3(BDC)_3(DPNO)_2$ only a short data collection was possible as the material rapidly changed colour from pink to brown with loss of crystallinity; given the instability of this material it was not studied any further. The magnesium material $Mg_2(BDC)_2(DPNDO)$ never formed crystals suitable for single X-ray diffraction, but powder X-ray diffraction was used to prove that it is isostructural with the cobalt analogue (Supporting Information), and a profile fit allowed refinement of its lattice parameters (spacegroup *P*2/*c*, *a* = 11.291(2) Å, *b* = 11.202(1) Å, *c* = 13.493(5) Å and β = 111.32(3) °), showing that the unit cell volume (1589.83 Å^3) is smaller than for $Co_2(BDC)_2(DPNDO)$ (1611.5 Å^3).

2. Thermal stability of $Co_2(BDC)_2(DPNDO)$ and $Mg_2(BDC)_2(DPNDO)$

Thermogravimetric analysis of $Co_2(BDC)_2(DPNDO)$ freshly prepared shows some initial mass losses below 400 °C, Figure 5, before final collapse of the materials with complete combustion

of the organic by 500 °C. After washing in methanol the initial mass loss occurs in one step: this corresponds to just more than 2 equivalents of methanol per $Co_2(BDC)_2(DPNDO)$ formula unit (expected 9.2 % mass loss; observed 11.6 %); alternatively the material may also contain some water as in the refined low temperature crystal structure (expected mass loss 14.4 %). (Note it is possible that the methanol and water content may vary from sample to sample, depending on atmospheric conditions and time.) The total overall mass loss at 900 °C of 78.6 % matches the expected total combustion to CoO of 78.5 % assuming 2 equivalents of methanol. For the as-made material the initial mass loss occurs in two distinct steps, suggesting two types of adsorbed species. Given that methanol was the major solvent used and the 1,4-benzenedicarboxylate (H_2BDC) was present in excess, the mass losses can be assigned assuming excess acid remains associated with the as-made material: the first loss is then due to 2 equivalents of methanol per $Co_2(BDC)_2(DPNDO)[H_2BDC]$ (expected 7.20 % mass loss and observed 7.95 %) followed by loss of 1 equivalent of unreacted H_2BDC (expected 23.06 % mass loss and observed 19.41 %). It is impossible to say whether the latter is absorbed in the pores or as a separate phase, although powder XRD suggests no bulk, crystalline H_2BDC is present. The fact that after washing the sample the methanol is lost in one step at low temperature corroborates the conclusion that the two-step mass loss seen for the as-made material is due to more than one adsorbed species, and the H_2BDC is removed by methanol washing. The methanol-washed sample of $Mg_2(BDC)_2(DPNDO)$ shows similar behaviour with first loss of at least 2 equivalents of methanol (and/or water) (expected 10.18 % for 2 methanol, observed 14.48 %) followed by combustion to MgO occurring at just above 400 °C (Supporting Information).

Thermodiffraction of $Co_2(BDC)_2(DPNDO)$, Figure 6 shows abrupt loss of crystallinity at 300 °C that would correspond to the collapse of the framework and linker combustion seen by TGA (note the different heating rate between the two experiments and the dwell time needed for the XRD means that the precise temperature of collapse may not be directly comparable). The change in intensity of the low angle peaks at the early stages of heating would be

consistent with loss of adsorbate molecules seen by TGA. Similar behaviour is seen for $Mg_2(BDC)_2(DPNDO)$ (Supporting Information). There is no evidence of 'breathing' behaviour prior to this collapse: the positions of Bragg peaks remain constant, implying there is no thermally induced flexibility in the structure from room temperature up to the point of collapse.

4. **Gas adsorption**

The simulated pore size distribution of the $Co_2(BDC)_2(DPNDO)$ structure (Supporting Information) indicates that its porosity may be considered to be a channel consisting of a series of small voids (4.9 Å in diameter) which are connected by smaller windows (3.8 Å in diameter), Figure 4a. The windows are defined by the edges of the BDC and DPNDO ligands, while the slightly larger regions of the pore system incorporate regions of space between neighbouring DPNDO ligands. The accessibility of these void spaces to different species has a considerable impact on light gas adsorption and the agreement between simulated and experimental adsorption isotherms depends strongly on both the polarity and size of the sorbate species but also on the temperature.

The permanent porosity of both materials was confirmed by gas-adsorption measurement on the methanol-washed samples. The N_2 adsorption isotherms at 77 K display a Type I sorption behavior (Supporting Information), verifying their microporous nature with an uptake capacity of 66 $cm^3\ g^{-1}$ and 78 $cm^3\ g^{-1}$ for $Co_2(BDC)_2(DPNDO)$ and $Mg_2(BDC)_2(DPNDO)$ at the saturation pressure, respectively. The standard BET analysis is performed for a pressure range of $0.05 < p/p_0 < 0.3$. However, microporous MOFs show saturation well below the standard range. To choose the pressure range appropriate for a particular adsorbent and to avoid ambiguity when reporting the BET surface area, two consistency criteria have been proposed: (1) the pressure range should be chosen so that $V_a*(1 - p/p_0)$ is always increasing with p/p_0 and (2) the straight line fitted to the BET plot must have a positive intercept. Taking into account these two criteria, the BET surface area were calculated to be 252 $m^2\ g^{-1}$ (p/p_0 = 0.0002-0.06) and 303 $m^2\ g^{-1}$ (p/p_0 = 0.0002-0.07) for $Co_2(BDC)_2(DPNDO)$ and $Mg_2(BDC)_2(DPNDO)$, respectively. The higher measured value for the isostructural Mg material

is consistent with its lower formula weight. The hysteresis observed in the nitrogen adsorption-desorption isotherms, although small, is reproducible and does not change on repeated measurements, suggesting it is a real effect and not due to structural collapse. This is supported by powder X-ray diffraction measured after the adsorption-desorption (Supporting Information), and also simulations (see below) that replicate the hysteretic behavior.

At 303 K, the adsorption of CO_2, CH_4 and N_2 is moderate and shows little selectivity, but the maximum uptake achieved is similar to other MOFs reported in the literature, such as the chromium(III) naphthalene tetracarboxylate MIL-102 (3-3.5 mmol.g^{-1} for CO_2, 1-1.5 mmol.g^{-1} for CH_4, 0.5-1 mmol.g^{-1} for N_2)[49] and $Sc_2(BDC)_3$ (3.5-4 mmol.g-1 for CO_2, 1.5-2 mmol.g^{-1} for CH_4, and 0.5-1 mmol.g^{-1} for N_2).[50] The shape of the adsorption isotherms is indicative of a microporous adsorbent. At low pressure (up to 3 bar), the filling of the pores leads to a relatively strong adsorption, followed by a plateau relative to the saturation of the microporous volume. The CO_2 adsorption is easily reversible: an evacuation step at 30°C is sufficient to regenerate fully the sample and a second adsorption cycle is essentially the same as the first. Interestingly, and unlike CO_2 and CH_4, with C_2H_6 an amount of adsorbed molecules could not be removed by simple vacuum at 30°C; this suggests a rather different interaction with this adsorbate (see below for further discussion of this when simulations are considered).

Two adsorption sites were identified in gas adsorption simulations for $Co_2(BDC)_2(DPNDO)$: one near the centre of the channel and another in the pockets of space between neighbouring DPNDO ligands, Figure 4a. There are four of these pocket sites per unit cell. In the case of nitrogen adsorption at 77 K (Figure 7), a stepped isotherm with a hysteresis loop is recovered from GCMC simulations. It is clear that these simulations vastly over-predict both the saturation capacity (6.4 mmol g^{-1}) and the BET surface area (457 m^2 g^{-1}) compared to experiment (3.4 mmol g^{-1} and 252 m^2 g^{-1}), a result of the different accessibilities of the pocket sites in simulation and in experiment. The initial plateau in the simulated isotherm corresponds to one nitrogen molecule in each of the pocket sites (4 molecules per unit cell in total) and a further 2 molecules per unit cell in the channel sites. The hysteresis loop is a result of the rearrangement of the adsorbed molecules in the channel sites to allow a further 2 molecules

per unit cell to be accommodated. If adsorption in the pocket sites is discounted in simulation (*i.e.* only adsorption in the channel is considered) then extremely good agreement with the experimental isotherm and the BET surface area is observed with a predicted surface area of 217 m^2 g^{-1}. These results indicate that the pocket sites are almost completely inaccessible to nitrogen at 77 K.

In the case of CH_4 and CO_2 adsorption at room temperature, reasonable agreement with experiment is obtained when both types of site are considered (Figure 8). For the non-polar but comparatively small methane molecule, simulations over-predict methane uptake suggesting that the pocket sites are less accessible in reality than in simulation. In the case of CO_2, simulations are able to capture the low pressure behaviour well but under-predict the saturation capacity. While the simulated isotherm is clearly Type I with a well-defined saturation capacity (4.0 mmol g^{-1}), the experimental CO_2 isotherm does not achieve saturation and it is possible that this is a result of the pocket sites becoming more accessible due to further distortion of the DPNDO linkers induced by a strong interaction between the polar CO_2 molecule and the MOF. This motion, and associated slight increase in accessible pore volume, is not accounted for in the GCMC simulations, which assume a completely rigid MOF.

Ethane is the largest of the guest molecules we have studied and comparatively poor agreement between simulation and experiment is observed for its adsorption isotherms at room temperature (Figure 8). At low pressure, the simulated uptake is much higher than observed in experiment. In simulation, the enhanced low pressure uptake at low pressure is driven primarily by adsorption in the relatively high-energy pocket sites and the comparatively low experimental uptake over the same pressure range indicates that these sites are initially inaccessible to ethane. The same pocket sites were accessible to CO_2 at low pressure, however, most likely a result of the increased polarity of CO_2 coupled with C_2H_6 having a larger critical molecular dimension. As the partial pressure of C_2H_6 is increased, the framework is distorted sufficiently to enable adsorption in these sites and a steady increase in ethane uptake is observed. As for CO_2, a Type I isotherm was not recovered experimentally and it appears that further distortion

of the framework enables more ethane to be adsorbed than predicted by the simulations, in which the MOF was assumed to be completely rigid.

5. Methanol uptake by $Co_2(BDC)_2(DPNDO)$ and $Mg_2(BDC)_2(DPNDO)$

Figure 9 shows thermogravimetric/DSC data recorded on pre-washed samples of the two materials as methanol is introduced. As shown by the TGA above, heating to 200 °C is enough to remove the already adsorbed methanol. After cooling to room temperature and exposure to a stream of methanol-saturated nitrogen both materials rapidly adsorb methanol to give almost the same mass as their initial state (note it is probable that the initial materials also had some surface-adsorbed methanol and/or water). This mass loss and gain in these experiments of ~10 %, corresponds to 2 methanols per $M_2(BDC)_2(DPNDO)$ formula unit (expected 9.17 % and 10.18 % for M = Co and Mg, respectively). Adsorption of methanol has a similar heat flow for both the Co and Mg materials; this is not unexpected since there are no open metal sites and the guest is being adsorbed into the pores with, presumably, the same guest-guest hydrogen-bonded interactions in each case. Note also the smaller event prior to methanol uptake and at the end of the experiment after release of methanol: this corresponds to a small uptake of water from the nitrogen carrier gas. The reversible uptake of methanol by microporous solids is of interest due to potential applications in low temperature heat transformation applications,[51] and although the mass uptake of methanol by $Mg_2(BDC)_2(DPNDO)$ is moderate at ~ 0.1 g g^{-1}, this was measured at ambient temperature and pressure so further investigation may be of interest.

Simulations suggest an uptake of methanol of ~ 15 wt% in $Co_2(BDC)_2(DPNDO)$ at room temperature, assuming a rigid MOF (Supporting Information), which corresponds to just under 6 molecules per unit cell. The same is true at 150 K (the capacity is unchanged, but the adsorption takes place at a much lower pressure). Thus the simulations over-predict the low temperature adsorption (the low temperature XRD of the methanol loaded structure showed 4 molecules per unit cell) but slightly over-predict capacity at room temperature. This supports the theory that there is some movement of the linker which affects the accessibility of the pocket

sites to small molecules. In the light of the thermodiffraction results given above, this structural flexibility is likely to be in response to the guest molecule, rather than solely thermally induced.

Conclusions

Using a combination of bidentate pyridine-*N*-oxide linkers and bidentate 1,4-benzene dicarboxylate linkers, two new metal-organic framework structures are synthesised for Co^{2+} and one prepared as an Mg^{2+} analogue. The material prepared using 2,2'-dipyridyl-*N*-oxide contains trimers of Co(II) centres with a 3-dimensional structure held together by only organic connectivity (I^0O^3), which may explain its thermal and X-ray sensitivity. In contrast, the bidentate 2,2'-dipyridyl-*N*,*N*'-dioxide (DPNDO) produces a 3-dimensional framework containing 1-dimensional *cis* and *trans* corner-shared chains of Co(II) octahedra (I^1O^2), which is a thermally robust structure from which residual solvent can be extracted to yield a microporous solid. The MOF thus produced shows moderate uptake of nitrogen, carbon dioxide and methane, but with no obvious selectivity towards any of these components. The measured gas adsorption isotherms are successfully simulated for these molecules assuming a rigid MOF structure, but in the case of the larger guest molecules ethane and methanol the measured adsorption isotherms are less well replicated. This suggests a more complex interaction between certain adsorbates and the MOF, which may involve guest and/or temperature induced flexibility.

Acknowledgements

The research leading to these results has received funding from the European Community's Seventh Framework Programme (FP7/2007-2013) under grant agreement No. 228862. Some of the equipment used in materials characterisation at the University of Warwick was obtained through the Science City Advanced Materials project "Creating and Characterising Next Generation Advanced Materials" with support from Advantage West Midlands (AWM) and part funded by the European Regional Development Fund (ERDF). We thank the EPSRC Crystallographic Service for recording one of the single crystal diffraction data sets and LMD thanks STFC and the Warwick EPSRC doctoral training account for funding.

Supporting Information

Further characterisation data: powder X-ray diffraction, thermogravimetry, nitrogen adsorption isotherms, and results of simulations. This material is available free of charge via the Internet at http://pubs.acs.org. Crystallographic data have been deposited with the Cambridge Crystallographic Data Centre (CCDC 1034971-1034973) and crystallographic information files can be obtained free of charge via www.ccdc.cam.ac.uk/data_request/cif.

References

(1) Burrows, A. D. *CrystEngCommun* **2011**, *13*, 3623-3642.

(2) Deng, H.; Doonan, C. J.; Furukawa, H.; Ferreira, R. B.; Towne, J.; Knobler, C. B.; Wang, B.; Yaghi, O. M. *Science* **2010**, *327*, 846-850.

(3) Kong, X.; Deng, H.; Yan, F.; Kim, J.; Swisher, J. A.; Smit, B.; Yaghi, O. M.; Reimer, J. A. *Science* **2013**, *341*, 882-885.

(4) Vermoortele, F.; Bueken, B.; Le Bars, G.; Van de Voorde, B.; Vandichel, M.; Houthoofd, K.; Vimont, A.; Daturi, M.; Waroquier, M.; Van Speybroeck, V.; Kirschhock, C.; De Vos, D. E. *J. Am. Chem. Soc.* **2013**, *135*, 11465-11468.

(5) Wu, H.; Chua, Y. S.; Krungleviciute, V.; Tyagi, M.; Chen, P.; Yildirim, T.; Zhou, W. *J. Am. Chem. Soc.* **2013**, *135*, 10525-10532.

(6) Fang, Z.; Durholt, J. P.; Kauer, M.; Zhang, W.; Lochenie, C.; Jee, B.; Albada, B.; Metzler-Nolte, N.; Poppl, A.; Weber, B.; Muhler, M.; Wang, Y.; Schmid, R.; Fischer, R. A. *J. Am. Chem. Soc.* **2014**, *136*, 9627-9636.

(7) Cliffe, M. J.; Wan, W.; Zou, X. D.; Chater, P. A.; Kleppe, A. K.; Tucker, M. G.; Wilhelm, H.; Funnell, N. P.; Coudert, F. X.; Goodwin, A. L. *Nat. Commun.* **2014**, *5*, 8.

(8) Ma, B. Q.; Mulfort, K. L.; Hupp, J. T. *Inorg. Chem.* **2005**, *44*, 4912-4914.

(9) P.Tomasik; Ratajewicz, Z.; Newkome, G. R.; Strekowski, L. In *Chemistry of Heterocyclic Compounds: Pyridine Metal Complexes*; John Wiley and Sons: 1985; Vol. Part 6, Volume 14, p 2068-2212.

(10) Sarma, R.; Perumal, A.; Baruah, J. B. *J. Coord. Chem.* **2009**, *62*, 1513-1524.

(11) Sarma, R.; Baruah, J. B. *Polyhedron* **2009**, *28*, 453-456.

(12) Sarma, R.; Boudalis, A. K.; Baruah, J. B. *Inorg. Chim. Acta* **2010**, *363*, 2279-2286.

(13) Sarma, R.; Baruah, J. B. *J. Coord. Chem.* **2010**, *63*, 457-463.

(14) Sarma, R.; Deka, H.; Boudalis, A. K.; Baruah, J. B. *Cryst. Growth Des.* **2011**, *11*, 547-554.

(15) Xu, G.; Zhang, X.; Guo, P.; Pan, C.; Zhang, H.; Wang, C. *J. Am. Chem. Soc.* **2010**, *132*, 3656-3657.

(16) Millange, F.; Serre, C.; Férey, G. *Chem. Commun.* **2002**, 822-823.

(17) Munn, A. S.; Clarkson, G. J.; Millange, F.; Dumont, Y.; Walton, R. I. *CrystEngCommun* **2013**, *15*, 9679-9687.

(18) Munn, A. S.; Clarkson, G. J.; Walton, R. I. *Acta Crystallogr. Sect. B* **2014**, *70*, 11-18.

(19) Luo, J.; Qiu, L. J.; Liu, B. S.; Gao, Y.; Zhang, X. R.; Yang, F.; Cui, L. L. *Chin. J. Chem.* **2011**, *29*, 905-912.

(20) Wang, Y. J.; Li, H. H.; Chen, Z. R.; Huang, C. C.; Huang, X. H.; Feng, M.; Lin, Y. *CrystEngCommun* **2008**, *10*, 770-777.

(21) Sarma, R.; Baruah, J. B. *Solid State Sci.* **2011**, *13*, 1692-1700.

(22) Coles, S. J.; Gale, P. A. *Chem. Sci.* **2012**, *3*, 683-689.

(23) Dolomanov, O. V.; Bourhis, L. J.; Gildea, R. J.; Howard, J. A. K.; Puschmann, H. *J. Appl. Cryst.* **2009**, *42*, 339-341.

(24) Sheldrick, G. M. *Acta Crystallogr. Sect. A* **2008**, *64*, 112-122.

(25) Wiersum, A. D.; Gioyannangeli, C.; Vincent, D.; Bloch, E.; Reinsch, H.; Stock, N.; Lee, J. S.; Chang, J.-S.; Llewellyn, P. L. *ASC Combin. Sci.* **2013**, *15*, 111-119.

(26) Lemmon, E. W.; McLinden, H. M. MO Reference Fluid Thermodynamic and Transport Properties; REFPROP 8.0; National Institute of Standards and Technology: Gaithersburg, MD, 2007.

(27) Gupta, A.; Chempath, S.; Sanborn, M. J.; Clark, L. A.; Snurr, R. Q. *Molecular Simulation* **2003**, *29*, 29-46.

(28) Peng, D.; Robinson, D. B. *Ind. Eng. Chem. Fundamen.* **1976**, *15*, 59-64.

(29) Mayo, S. L.; Olafson, B. D.; Goddard, W. A. *J. Phys. Chem.* **1990**, *94*, 8897-8909.

(30) Rappe, A. K.; Casewit, C. J.; Colwell, K. S.; Goddard, W. A.; Skiff, W. M. *J. Am. Chem. Soc.* **1992**, *114*, 10024-10035.

(31) Wilmer, C. E.; Kim, K. C.; Snurr, R. Q. *J. Phys. Chem. Lett.* **2012**, *3*, 2506-2511.

(32) Martin, M. G.; Siepmann, J. I. *J. Phys. Chem. B* **1998**, *102*, 2569-2577.

(33) Potoff, J. J.; Siepmann, J. I. *AICHE J.* **2001**, *47*, 1676-1682.

(34) Brese, N. E.; O'Keeffe, M. *Acta Crystallogr. Sect. B* **1991**, *47*, 192-197.

(35) Poulsen, R. D.; Bentien, A.; Christensen, M.; Iversen, B. B. *Acta Crystallogr. Sect. B* **2006**, *62*, 245-254.

(36) Clausen, H. F.; Overgaard, J.; Chen, Y. S.; Lversen, B. B. *J. Am. Chem. Soc.* **2008**, *130*, 7988-7996.

(37) Luo, F.; Che, Y. X.; Zheng, J. M. *Cryst. Growth Des.* **2009**, *9*, 1066-1071.

(38) Zhang, J.; Bu, J. T.; Chen, S.; Wu, T.; Zheng, S.; Chen, Y.; Nieto, R. A.; Feng, P.; Bu, X. *Angew. Chem., Int. Ed.* **2010**, *49*, 8876-8879.

(39) Wang, X. F.; Zhang, Y. B.; Xue, W.; Qi, X. L.; Chen, X. M. *CrystEngCommun* **2010**, *12*, 3834-3839.

(40) Zou, H.-H.; He, Y.-P.; Gui, L.-C.; Liang, F.-P. *CrystEngCommun* **2011**, *13*, 3325-3329.

(41) Cheetham, A. K.; Rao, C. N. R.; Feller, R. K. *Chem. Commun.* **2006**, 4780-4795.

(42) Harvey, H. G.; Slater, B.; Attfield, M. P. *Chem, Eur. J.* **2004**, *10*, 3270-3278.

(43) Harvey, H. G.; Teat, S. J.; Attfield, M. P. *J. Mater. Chem.* **2000**, *10*, 2632-2633.

(44) Yuan, Z. H.; Clegg, W.; Attfield, M. P. *J. Porous Mat.* **2006**, *13*, 207-212.

(45) Yang, S.; Sun, J.; Ramirez-Cuesta, A. J.; Callear, S. K.; David, W. I. F.; Anderson, D. P.; Newby, R.; Blake, A. J.; Parker, J. E.; Tang, C. C.; Schroeder, M. *Nat. Chem.* **2012**, *4*, 887-894.

(46) Lin, Q.; Wu, T.; Zheng, S.-T.; Bu, X.; Feng, P. *Chem. Commun.* **2011**, *47*, 11852-11854.

(47) Qian, J.; Jiang, F.; Yuan, D.; Wu, M.; Zhang, S.; Zhang, L.; Hong, M. *Chem. Commun.* **2012**, *48*, 9696-9698.

(48) Spek, A.L. *Acta Crystallogr., Sec. D* **2009**, *65*, 148-155.

(49) Surblé, S.; Millange, F.; Serre, C.; Duren, T.; Latroche, M.; Bourrelly, S.; Llewellyn, P. L.; Férey, G. *J. Am. Chem. Soc.* **2006**, *128*, 14889-14896.

(50) Miller, S. R.; Wright, P. A.; Devic, T.; Serre, C.; Férey, G.; Llewellyn, P. L.; Denoyel, R.; Gaberova, L.; Filinchuk, Y. *Langmuir* **2009**, *25*, 3618-3626.

(51) Jeremias, F.; Froehlich, D.; Janiak, C.; Henninger, S. K. *New J. Chem.* **2014**, *38*, 1846-1852.

Table 1: Crystal Structure Data for $Co_3(BDC)_3(DPNO)_2$ and $Co_2(BDC)_2(DPNDO)$

	$Co_3(BDC)_3(DPNO)_2$	$Co_2(BDC)_2(DPNDO)$	$Co_2(BDC)_2(DPNDO)[CH_3OH]_{2.5}[H_2O]_{1.5}$
Formula	$C_{44}H_{28}Co_3N_4O_{14}$	$C_{26}H_{16}Co_2N_2O_{10}$	$C_{27.25}H_{22.50}Co_2N_2O_{12}$
Data Collection	Rigaku Saturn724+ (Mo Kα)	Oxford Diffraction Gemini R (Mo Kα)	Oxford Diffraction Gemini R (Mo Kα)
Temperature / K	100	296	150
Crystal System	triclinic	monoclinic	triclinic
Space Group	$P\bar{1}$	$P2/c$	$P\bar{1}$
a / Å	9.650(6)	11.3517(12)	11.3407(5)
b / Å	17.270(12)	11.3956(10)	11.3847(9)
c / Å	18.274(12)	13.2806(12)	13.1908(7)
α / °	99.057(11)	90	88.868(6)
β/ °	90.485(9)	110.274(11)	69.339(5)
γ/ °	106.122(10)	90	85.726(5)
V / Å^3	2885(3)	1611.5(3)	1589.07(18)
Z	2	2	2
μ (Mo Kα) / mm^{-1}	0.926	1.079	1.105
Crystal size / mm^3	0.05 x 0.04 x 0.01	0.2 x 0.06 x 0.04	0.2 x 0.06 x 0.04
R_{int}	0.136	0.116	0.103
Reflections measured, unique	37606, 13070	22037, 13479	34873, 13810
GOF on F^2	0.989	1.492	0.962
$R1$, w$R2$ [$I > 2\sigma(I)$]	0.0898, 0.2484	0.1108, 0.2568	0.0738, 0.1089
Data / restraints / parameters	13070/ 42/ 589	13479/121/380	13810/0/184
Largest peak, hole / e·Å^{-3}	0.744, -1.135	1.81, -1.53	2.07, -1.32

Figure Captions

Figure 1: The bidentate pyridine-*N*-oxide ligands used as co-ligands in this work: 2,2'-dipyridyl-*N*-oxide (DPNO) and 2,2'-dipyridyl-*N*,*N*'-dioxide (DPNDO).

Figure 2: Views of the structure of $Co_3(BDC)_3(DPNO)_2$: (a) the local connectivity of trimeric units and (b) view along the *a*-axis showing the one-dimensional channels and the pillared layered nature of the structure. The Co4-Co1-Co4 trimer units shown as blue polyhedra and Co3-Co2-Co3 as green, carbon atoms are pale grey, oxygen red and nitrogen blue; hydrogen atoms are not shown for clarity. The incomplete bonds are part of BDC linkers that connect to other similar trimers.

Figure 3: Views of the structure of $Co_2(BDC)_2(DPNDO)$: (a) part of one of the infinite chains running approximately along *c* and (b) view along *a* showing the connectivity of the chains. Carbon atoms are pale grey, oxygen red and nitrogen blue; hydrogen atoms are not shown for clarity. The incomplete bonds are part of BDC linkers that connect to other similar chains.

Figure 4: Views of the structure of $Co_2(BDC)_2(DPNDO)$ determined at (a) room temperature and (b) 150 K with adsorbed methanol, showing one-dimensional channels running along the *c* axis. Carbon atoms are pale grey, oxygen red and nitrogen blue; hydrogen atoms are not shown for clarity. In (a), the main channel of the pore (diameter 3.8 Å) and void spaces near the DPNDO ligands (diameter 4.9 Å) are indicated by orange and green spheres respectively. In (b) the methanol sites with the highest occupancy are shown; as discussed in the text there are also lower occupied methanol and water sites in the pores.

Figure 5: Themogravimetric analysis of $Co_2(BDC)_2(DPNDO)$ (static air, heated at 10 °C min^{-1})

Figure 6: Thermodiffraction showing the effect of heating in air upon $Co_2(BDC)_2(DPNDO)$

Figure 7: Nitrogen adsorption (filled symbols) and desorption (empty symbols) isotherms at 77 K in $Co_2(BDC)_2(DPNDO)$. The experimental points are shown by green triangles while simulations in which both pocket and channel sites were considered are shown as blue diamonds and in which only the channel sites were considered are shown as red diamonds.

Figure 8: Simulated (filled symbols) and experimental (empty symbols) adsorption isotherms for CO_2 (green triangles), CH_4 (blue diamonds) and C_2H_6 (red squares) at 303 K in $Co_2(BDC)_2(DPNDO)$

Figure 9: Gravimetric analysis of methanol adsorption from the vapour phase. Nitrogen saturated with methanol was flowed over the samples from 7000 to 12500 s; otherwise nominally dry nitrogen was used.

For Table of Contents Use Only

Metal-Organic Frameworks from Divalent Metals and 1,4-Benzenedicarboxylate with Bidentate Pyridine-N-oxide Co-ligands

Alexis S. Munn, Silvia Amabilino, Thomas W. Stevens, Luke M. Daniels, Guy J. Clarkson, Franck Millange, Matthew J. Lennox, Tina Düren, Sandrine Bourelly, Philip Llewellyn and Richard I. Walton

Two new MOF structures are synthesised from a combination of bidentate dicarboxylate and bidentate pyridine-*N*-oxide ligands; using 1,4-benzenedicarboxylate and 2,2'-dipyridyl-*N*,*N*'-dioxide (DPNDO) gives a solid that contains infinite inorganic chains of octahedral divalent metals (Co^{2+} or Mg^{2+}) that is thermally robust and permanently porous towards small adsorbate molecules such as methane, carbon dioxide, nitrogen and methanol.

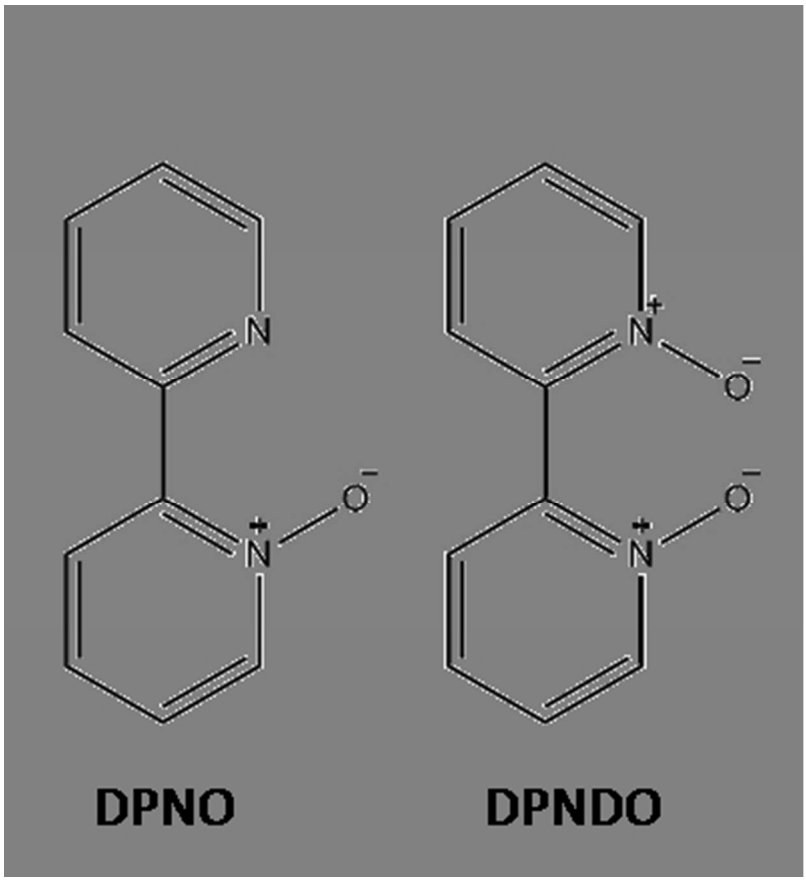

67x73mm (150 x 150 DPI)

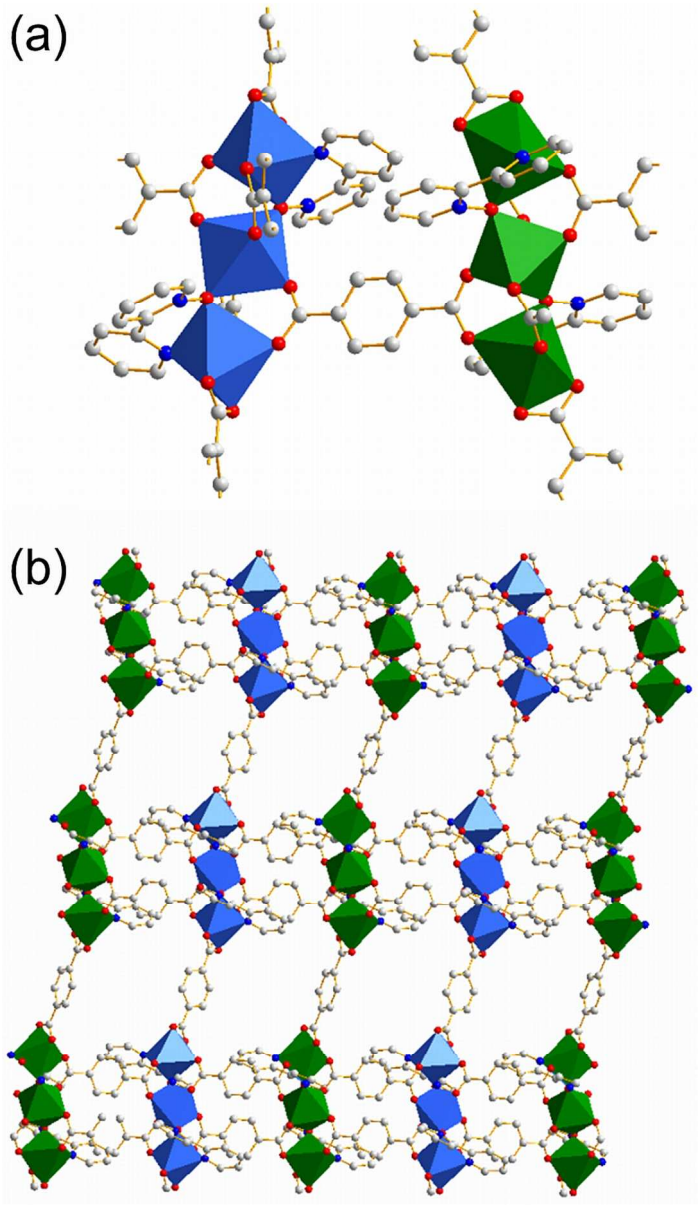

82x142mm (300 x 300 DPI)

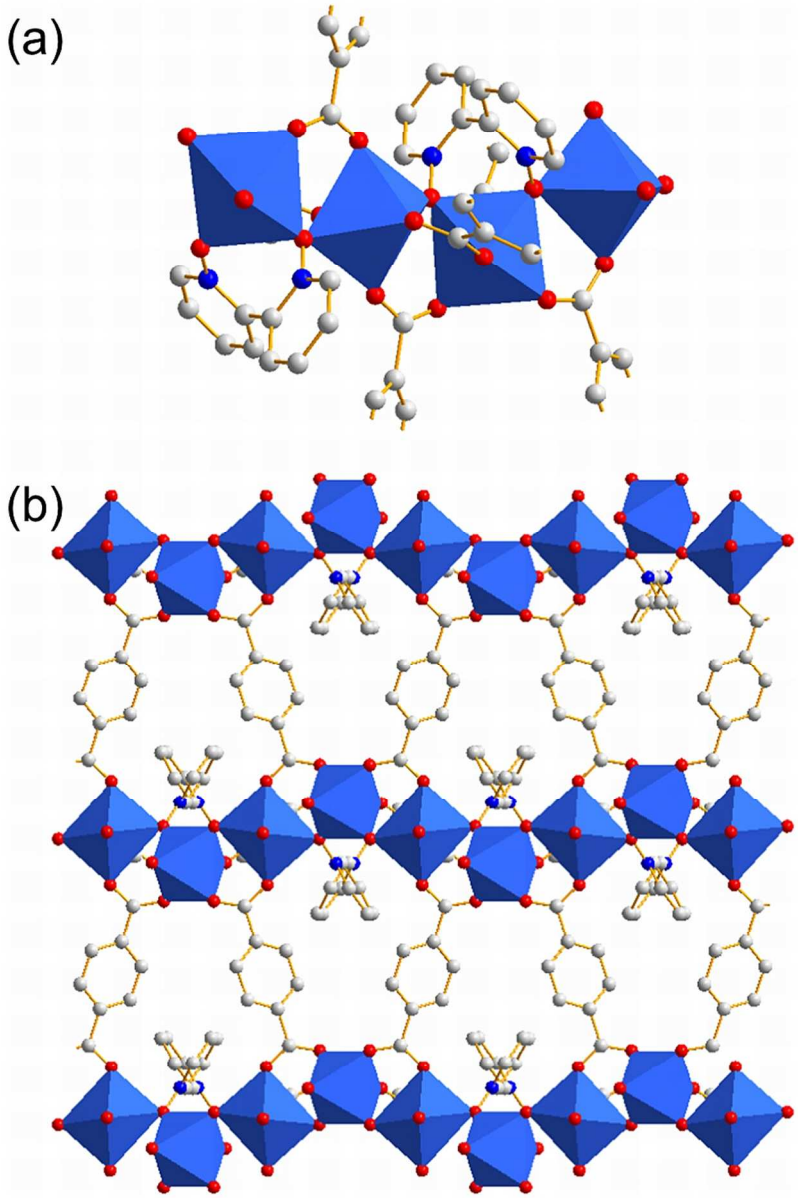

82x124mm (300 x 300 DPI)

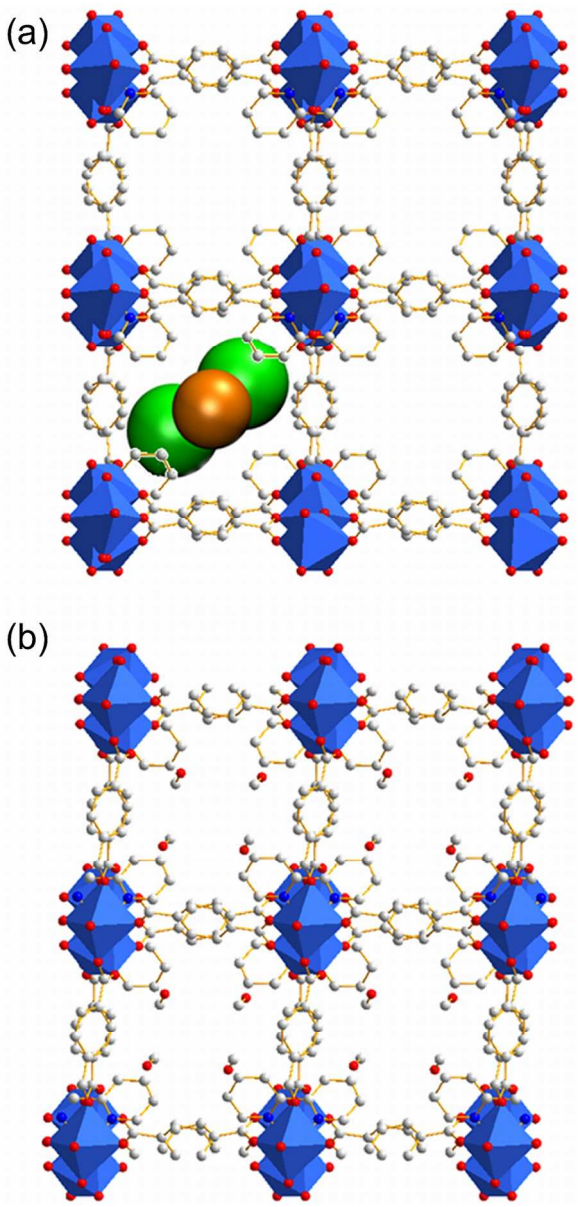

82x171mm (300 x 300 DPI)

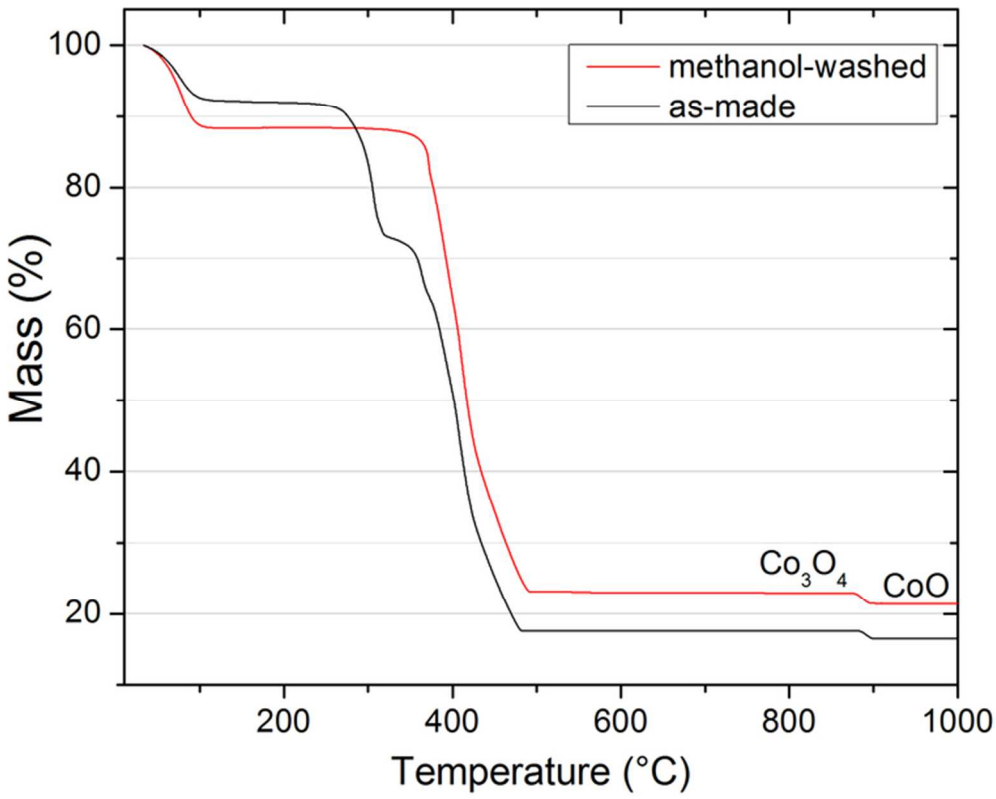

64x51mm (300 x 300 DPI)

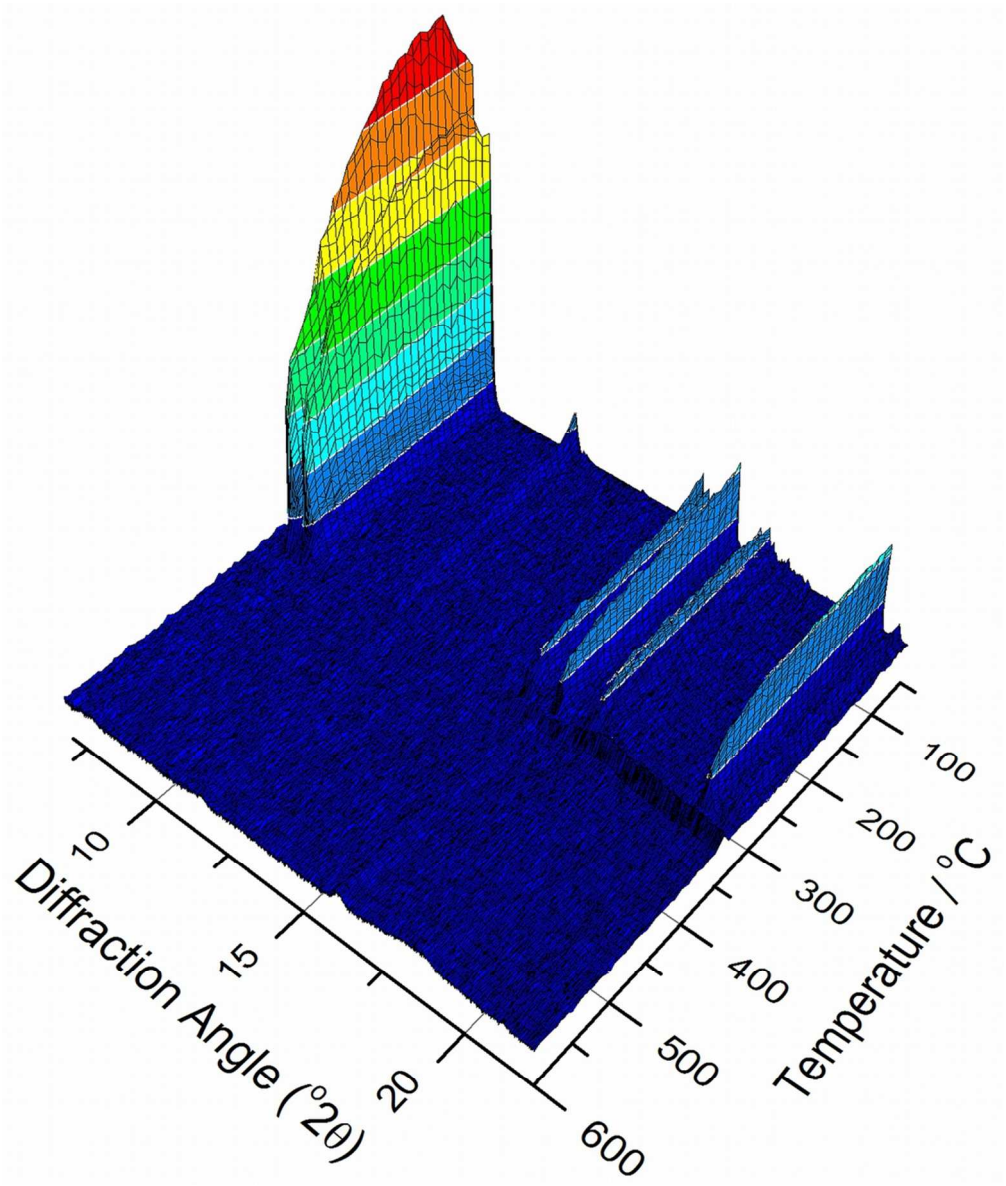

97x114mm (300 x 300 DPI)

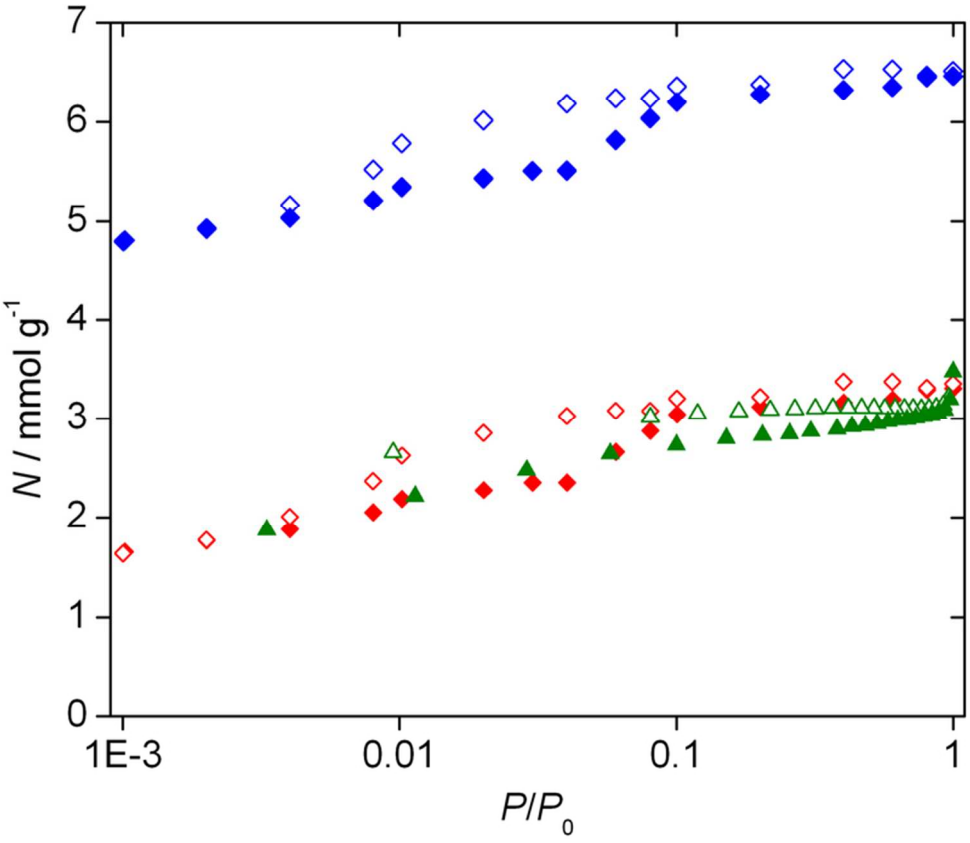

69x59mm (300 x 300 DPI)

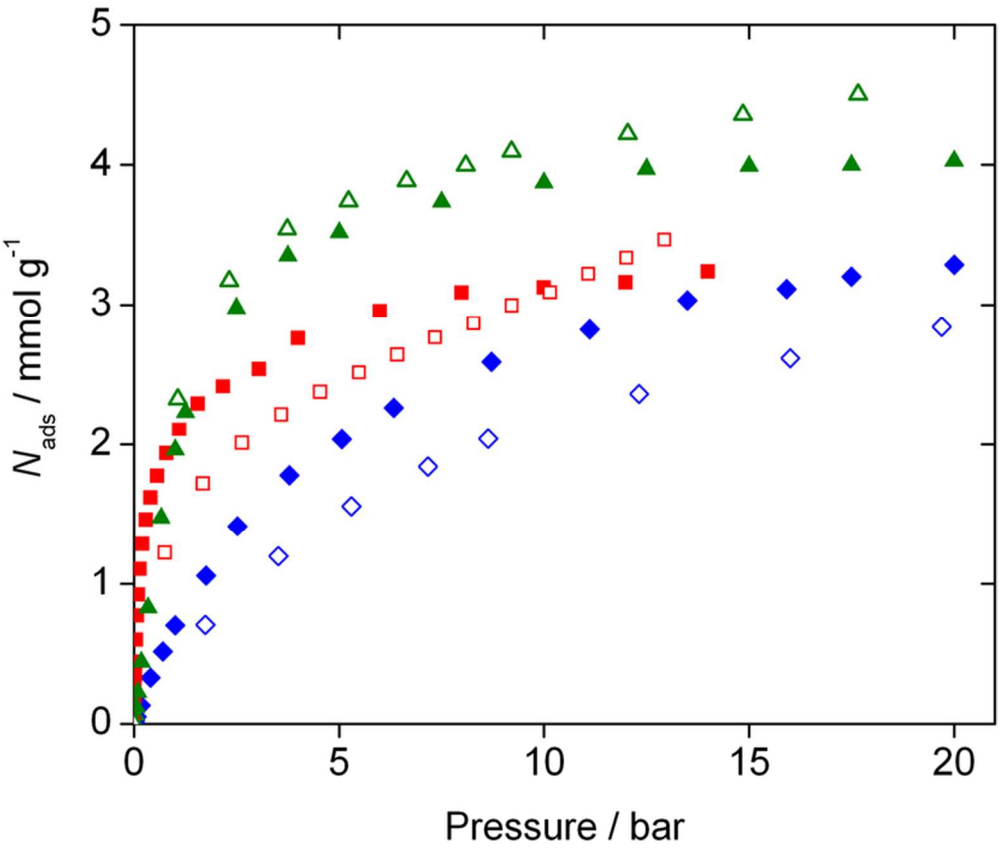

70x60mm (300 x 300 DPI)

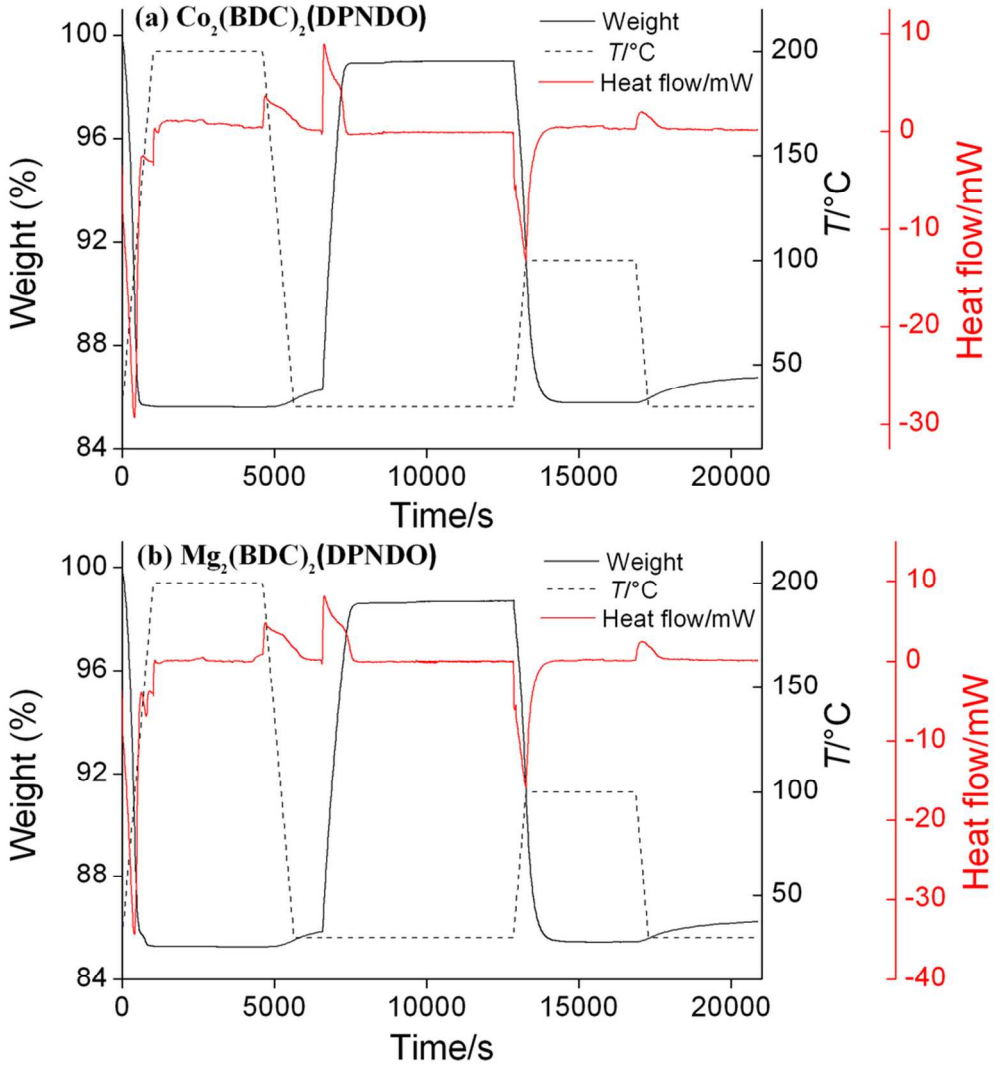

88x95mm (300 x 300 DPI)

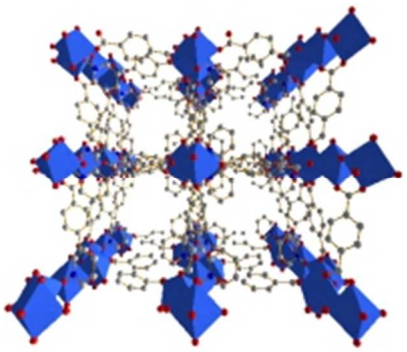

53x46mm (96 x 96 DPI)